BIOCHEMISTRY
including biophysical chemistry & molecular biology
Article

Biochemistry **2009,** *48,* 10255–10266 10255
DOI: 10.1021/bi900666n

Kinetic Mechanism and Inhibitor Characterization of WNK1 Kinase

Yukiko I. Yagi,* Koichi Abe, Kazunori Ikebukuro, and Koji Sode

Tokyo University of Agriculture and Technology, 2-24-16 Naka-machi, Koganei, Tokyo, Japan

Received April 18, 2009; Revised Manuscript Received September 6, 2009

ABSTRACT: Pseudohypoaldosteronism type II (PHAII) is caused by the mutation of two members of the WNK (with-no-K[Lys] kinase) kinase family. We describe here the development of an in vitro WNK1 microfluidic mobility shift assay for kinetic mechanism studies. Assays using capillary electrophoresis on a microfluidic chip are suitable for both compound selection and mechanistic studies, because of the robustness of this method, as well as its high-throughput feature and insensitivity to the ATP concentration. Double-reciprocal plots of the initial rates versus the concentration of the substrate revealed that the random sequential activity of WNK catalyzed OXSR1 (oxidative stress response kinase-1) phosphorylation. WNK1 inhibitors were then found from among 86 kinases in a commercially available library. Interestingly, the Hck, Lck, and Src inhibitors, PP1 and PP2, exhibited positive inhibition against WNK1. The inhibition mode of PP1 was analyzed to be pure ATP competition with a K_i value of 12.7 μM, showing noncompetitive inhibition against the OXSR1 peptide. From the structure-based comparison, we found that, since the WNK1 enzymes are categorized as STEs (homologues of yeast Sterile 7, Sterile 11, and Sterile 20 kinases) and Hck belongs to the TK (tyrosine kinase) family on the basis of the results of the Human Kinome Project, the residues at the catalytic site of the WNK1 that interact with PP1 were well-conserved in Hck. We concluded that the compound-based structural alignment enabled us to find interesting relationships among the kinases. This information helps us to screen specific WNK1 therapeutic reagents with no inhibition of the Src, Hck, and Lck kinases for the treatment of hypertension.

WNK1 (with-no-K[Lys] kinase-1) and WNK4 were identified as genes mutated in the families of patients with pseudohypoaldosteronism type II (PHAII) human hypertension (*1*, *2*). Pseudohypoaldosteronism type II (Online Mendelian Inheritance in Man database entry 145260) is an autosomal dominant disease featuring hypertension with hyperkalemia despite a normal glomerular filtration rate. PHAII patients are treated with thiazide diuretics, which function as antagonists of the Na^+/Cl^- cotransporter (NCC),[1] suggesting that the activity of NCC could be related to PHAII.

There are four isoforms of WNK (WNK1, -2, -3, and -4) in humans encoded by distinct genes (*3*). Genetic studies in humans have shown that large intronic deletions in WNK1 lead to its overexpression and are responsible for the onset of PHAII (*4*). Consistent with human genetic studies, WNK1 heterozygous mice displayed a significant decrease in blood pressure (*5*). In contrast, mutations in the WNK4 gene are found in the coding sequence near the coiled-coil domains (E562K, D564A, and Q565E). It is not yet clear how mutations in WNK4 lead to PHAII, but in $WNK4^{PHA}$-transgenic mice and $WNK4^{D561A/+}$ knockin mice, the blood pressure was increased (*6*, *7*). Recently, evidence that the WNK1-SPAK/OXSR1-NKCC/NCC signaling pathway plays a key role in controlling the blood pressure has been reported (*8*, *9*). WNK1 and WNK4 interact with STE20/SPS1-related proline alanine-rich kinase (SPAK) and oxidative stress response kinase-1 (OXSR1) (*10*−*12*). Human SPAK and OXSR1 consist of an N-terminal catalytic domain belonging to the STE20 kinase subfamily, and a conserved C-terminal (CCT) domain, which interacts with the RFXV/I motifs present in WNK1/4, NKCC1, and NCC (*12*−*15*). In vitro, WNK1 kinase activates SPAK and OXSR1 (*8*, *11*, *14*) by phosphorylating a Thr residue (Thr233 of SPAK and Thr185 of OXSR1) and a Ser residue (Ser373 of SPAK and Ser325 of OXSR1) (*11*). The activated SPAK and OXSR1 interact, phosphorylate, and activate the $Na^+/K^+/2Cl^-$ cotransporter (NKCC1) (*13*, *16*) and Na^+/Cl^- cotransporter (NCC) (*9*). In the mammalian cell, hyperosmotic (*8*) and hypotonic low-chloride conditions (*14*) cause the phosphorylation of WNK1, a change in its cellular localization from the cytosol to vesicles (*17*), and an increase in the extent of activation of the WNK1-SPAK/OXSR1-NKCC1 pathway (*8*, *14*, *17*). Recent findings indicate that SPAK and OXSR1 interact with NCC and phosphorylate three residues in human NCC (Thr46, Thr55, and Thr60) following the activation of the WNK1-SPAK/OXSR1 pathway induced by hypotonic

*To whom correspondence should be addressed. Phone and fax: +81-42-388-7073. E-mail: 50006831703@st.tuat.ac.jp.

[1]Abbreviations: AIC, Akaike's information criterion; Av, average; CV, coefficient of variation; DMSO, dimethyl sulfoxide; DTT, dithiothreitol; FAM, 5′-carboxyfluorescein; IC_{50}, inhibitor concentration at 50% inhibition; KD, kinase domain; K_i, equilibrium dissociation constant; K_m, Michaelis−Menten constant; SC_{50}, substrate concentration yielding 50% of the maximal rate of the enzyme reaction; MOA, mode of action; OSR1/OXSR1, oxidative stress response kinase-1; QA, quality assurance; QC, quality control; S/B, signal-to-background ratio; SD, standard deviation; SPAK, STE20/SPS1-related proline alanine-rich kinase; Tris, 2-amino-2-(hydroxymethyl)-1,3-propanediol; Tween 20, polyoxyethylene sorbitan monolaurate; V_{max}, maximum initial velocity (maximal rate of the enzyme-catalyzed reaction); WNK, with-no-Lys kinase; Z' factor, measure of the quality or power of a high-throughput screening (HTS) assay; KD, kinase domain; NKCC1, $Na^+/K^+/2Cl^-$ cotransporter; NCC, Na^+/Cl^- cotransporter; EGFR, epidermal growth factor receptor; Hck, hemopoietic cell kinase; Lck, lymphocyte cell-specific protein-tyrosine kinase; Src, proto-oncogene tyrosine-protein kinase; ZAP-70, 70 kDa ζ-associated protein; Jak2, Janus kinase 2; PKA, cAMP-dependent protein kinase; JNK, Jun N-terminal kinase.

Published on Web 09/09/2009

low-chloride stress (*9*). These recent findings suggest that WNK kinase is involved in hypertension.

Of great interest is the unique active site of WNK1 kinase. This site contains a cysteine in place of lysine at the usual conserved location of the ATP binding site (*18*). WNK1 contains an N-terminal kinase domain (residues 221−479), three putative coiled-coil domains, and RFXV motifs, which could interact with the CCT domains of the substrate kinases (*3*, *15*, *19*−*21*). The crystal structure of the kinase domain of WNK1 indicates that there is a lysine residue (Lys233) at the active site emanating from strand β2 (subdomain I) rather than strand β3 (subdomain II), in contrast to the situation for other kinases (*22*).

Understanding the detailed kinetic mechanism of an enzyme is necessary for the development of specific inhibitors (*23*, *24*). To better grasp the mechanism of the WNK1 enzyme reaction, we established a WNK1 enzyme assay based on the microfluidic-based mobility shift assay. Currently, there are many homogeneous-type kinase assays in use, each with advantages and drawbacks. Four commonly used assay technologies are the radioactivity-based assay [SPA (scintillation proximity assay) (GE Healthcare) (*25*)], the antibody-based fluorescence assay [HTRF (homogeneous time-resolved fluorescence) (Cis-Bio, Bagnols-sur-Cèze, France), AlphaScreen (amplified luminescent proximity homogeneous assay) (PerkinElmer, Boston, MA), and LANCE (lanthanide chelate excitation) (PerkinElmer) (*26*, *27*)], the fluorescence polarization-based assay [IMAP (immobilized metal ion affinity-based fluorescence polarization) (Molecular Devices Corp., Sunnyvale, CA) (*28*)], and the mobility shift-based assay (Caliper Life Sciences, Inc., Hopkinton, MA) (*29*, *30*). The radioactivity-based SPA uses [^{33}P]ATP or [^{32}P]ATP labeled at the γ-phosphate. Upon kinase catalysis, the γ-phosphate is transferred from the ATP to the substrate. While this method is sensitive, it requires special precautions and equipment for handling the radioactivity. Furthermore, it is difficult to develop radiometric assays at high concentrations of ATP, as increasing concentrations of radiolabeled ATP lead to an increased background, making it difficult to identify the inhibitor mode of action (*31*). Antibody-based fluorescence assays (HTRF, AlphaScreen, and LANCE) use phospho-specific antibodies, in conjunction with various other fluorescence technologies, to detect the phosphorylated products of the kinase reaction. This method is suitable for the analysis of the inhibitor mode of action because there is no upper limit on the ATP concentration. However, assay development depends on the availability of a phospho-specific antibody. There was no available phospho-OXSR antibody; therefore, it was difficult to develop antibody-based fluorescence assays for WNK1. The fluorescence polarization-based assay (IMAP) uses metal-derivatized nanoparticles to replace phospho-specific antibodies for detection. These particles are coated with metal ions (M^{3+}) that can bind to the fluorescein-labeled phospho-peptide substrate, leading to an increase in FP. There is one commercially available IMAP-based WNK1 assay; however, it cannot tolerate high ATP concentrations. Because ATP contains a phosphate group, it competes with the product in binding to the metal ion, thus making compound ATP competitiveness studies impossible (*32*, *33*). The IMAP detection reagents stop the reaction by lowering the pH and by binding to the remaining ATP; thus, real-time kinetics cannot be determined. Therefore, we need to establish a novel WNK1 enzyme assay to evaluate the enzymatic characteristics and inhibitor mode of action of WNK1. The mobility shift-based assay is marketed by Caliper Life Sciences, Inc. This technology relies on a shift in mobility within an electric field between the fluorescein-labeled peptide substrate and its phosphorylated product. The product and substrate are quantified by fluorescence detection on a microfluidic chip (*34*). Because the Caliper-based enzyme assay has no upper limit on how much ATP can be used, it is possible to determine the kinetic mechanism at various concentrations of ATP. It also allows us to determine the IC_{50} value while maintaining a high ATP concentration, like that found under cellular conditions (in the millimolar range). The unique feature of this technology was formerly applied to assays for the lipid-modifying enzyme (*35*), protein kinase B (PKB/AKT) from cell lysate (*29*), DNA polymerase (*36*), and phosphatase (*30*).

In this work, we developed a WNK1 enzyme assay using the mobility shift-based assay. The kinetic mechanism of WNK1 and the results of compound mechanistic studies thereon are described here for the first time.

MATERIALS AND METHODS

Materials. For the enzyme assay, the GST-WNK1(1−491) enzyme was purchased from Carna Biosciences (Kobe, Japan). The OXSR1 peptide was synthesized by Toray Research Center, Inc. (Tokyo, Japan). White solid low-volume plates were purchased from Corning (Acton, MA). Dithiothreitol (DTT) was from Wako Pure Chemical Industries, Ltd. (Osaka, Japan). ATP, AMP-PNP, and dimethyl sulfoxide (DMSO) Hybri-Max were from Sigma-Aldrich (St. Louis, MO). The LabChip3000 instrument was from Caliper Life Sciences, Inc., and the Screen-Well Kinase Inhibitor Library was from BIOMOL International (Plymouth Meeting, PA).

WNK Mobility Shift Assay. A mixture of fluorescein-labeled OXSR1 peptide substrate (Toray Research Center, Inc.) and ATP was prepared with final concentrations of 10 and 25 μM, respectively, in 7 μL of reaction buffer [20 mM HEPES-Na (pH 7.5), 1 mM $MnCl_2$, 0.01% Tween 20, and 2 mM DTT]. A dosed compound at a final concentration from 0.003 to 100 μM in 1 μL was added to the peptide/ATP mixture at a final DMSO concentration of 10%. The reaction was started by the addition of 2 μL of GST-WNK1(1−491) (Carna Biosciences) that was 86% pure at a final concentration of 25 nM in a 384-well plate. After incubation for 3 h at 25 °C, 10 μL of a stop buffer containing 0.2% coating-3 reagent with 2 mM EDTA was added. For 800 μM ATP, the WNK1 was reacted for 50 min at 25 °C. Aliquots from each well were sipped onto a four-sipper chip on a Labchip3000 instrument for electrophoretic separation of the substrate, and the fluorescence intensity was measured under a pressure of −2.0 psi and a voltage of −1650 ΔV. The relative peak heights of the substrate and product were measured, and the peak ratio was calculated using HTS Well Analyzer version 4.1. The ratio was defined as the height of the product peak divided by the sum of the peak heights of the product and the substrate. Calibration was done using the low control, i.e., the enzyme reaction in the presence of 2 mM EDTA, and the high control, i.e., the enzyme reaction in the absence of EDTA. The percentage of inhibition was calculated as follows:

$$\%\ \text{inhibition} = 100[1 - (r - r_{\text{low control}})/(r_{\text{high control}} - r_{\text{low control}})]$$

where r, $r_{\text{low control}}$, and $r_{\text{high control}}$ are the peak ratios for the tested compound, the low control, and the high control, respectively. For the kinetic analysis, 21 μL of fluorescein-labeled OXSR1 peptide (0−40 μM) and ATP (0−800 μM), both at

various concentrations, was incubated with 3 μL of DMSO in the reaction buffer containing 20 mM HEPES-Na (pH 7.5), 1 mM $MnCl_2$, 0.01% Tween 20, and 2 mM DTT. The reaction was started by the addition of 6 μL of the enzyme at a final concentration of 25 nM in the 384-well plate (Corning). The plate was placed immediately in the Labchip 3000 system, and the samples were sipped onto a four-sipper chip every 3 min from 90 to 250 min. The temperature and humidity in the reaction chamber were maintained at 20 °C and 50%, respectively. The substrates and phosphorylated products were separated and detected on the chip. The initial velocity versus each substrate concentration was determined for calculation of the K_m value for the ATP and the peptide substrate.

Dynamic Range of the WNK1 Mobility Shift Assay. The fluorescein-labeled OXSR1 peptide substrate was prepared at a final concentration of 0−10 μM, in reaction buffer [20 mM HEPES-Na (pH 7.5), 1 mM $MnCl_2$, 0.01% Tween 20, and 2 mM DTT]. The fluorescence intensity was measured on a Labchip 3000 instrument. Aliquots (6 μL) of the WNK1 solution in the reaction buffer system were added to a 384-well plate (Corning) containing 24 μL of the ATP (25, 800 μM)/OXSR1 (10 μM) substrate peptide in reaction buffer. The plate was placed immediately in the Labchip 3000 system, and the samples were sipped onto a four-sipper chip every 3 min from 0 to 60 min. The temperature and humidity in the reaction chamber were maintained at 20 °C and 50%, respectively. The substrates and phosphorylated products were separated and detected on the chip. The initial velocity versus each WNK1 concentration was determined for calculation of the linear regression standard curve.

Kinetic Data Analysis. The initial rate data from the WNK1-catalyzed two-substrate kinetic profiles were fitted to eq 1(sequential, ordered bi-bi mechanism), eq 2 (sequential, random bi-bi mechanism), and eq 3 (ping-pong bi-bi mechanism) using SigmaPlot Enzyme Kinetics Module (Systat Software, Inc., San Jose, CA):

$$v = V_{max}[A][B]/(K_{ia}K_{mB} + K_{mB}[A] + K_{mA}[B] + [A][B]) \quad (1)$$

$$v = V_{max}[A][B]/(K_{mA}K_{mB} + K_{mB}[A] + K_{mA}[B] + [A][B]) \quad (2)$$

$$v = V_{max}[A][B]/(K_{mB}[A] + K_{mA}[B] + [A][B]) \quad (3)$$

where V_{max} is the maximum initial velocity, A and B represent the substrates, K_{ia} is the constant of dissociation of substrate A from the free enzyme, and K_{mA} and K_{mB} are the corresponding Michaelis−Menten constants for A and B, respectively. To define the mechanism of WNK1 inhibition, the inhibition assay was conducted by keeping one substrate at a fixed concentration, while the concentration of the other substrate was varied in the absence or presence of the inhibitor at various concentrations. When ATP was the varied substrate, the concentration of fluorescein-labeled OXSR1 was fixed at 10 μM, and when fluorescein-labeled OXSR1 was the varied substrate, the concentration of ATP was fixed at 50 μM. For the inhibition experiments, the concentration of staurosporine and phospho-OXSR1 peptide ranged from 0 to 170 μM, that of tyrphostin 47 ranged from 0 to 12 μM, those of PP1 and PP2 ranged form 0 to 25 μM, and that of AMP-PNP ranged from 0 to 245 μM. By using the SigmaPlot Enzyme Kinetics Module (Systat Software, Inc.), the initial velocities were automatically fitted to the equations, and the best-fit inhibition model was identified from among the complete competitive (eq 4), partial competitive (eq 5), complete noncompetitive (eq 6), partial noncompetitive (eq 7), complete uncompetitive (eq 8), partial uncompetitive (eq 9), complete mixed (eq 10), and partial mixed (eq 11) models.

$$v = V_{max}/[1 + (K_m/[S])(1 + [I]/K_i)] \quad (4)$$

$$v = V_{max}/[1 + (K_m/[S])(1 + [I]/K_i)/(1 + [I]/\alpha K_i)] \quad (5)$$

$$v = V_{max}/[(1 + [I]/K_i)(1 + K_m/[S])] \quad (6)$$

$$v = V_{max}/[(1 + K_m/[S])(1 + [I]/K_i)/(1 + [I]\beta/K_i)] \quad (7)$$

$$v = V_{max}/(1 + [I]/K_i + K_m/[S]) \quad (8)$$

$$v = V_{max}[1 + \beta([I]/K_i)]/(1 + [I]/K_i + K_m/[S]) \quad (9)$$

$$v = V_{max}/[(K_m/[S])(1 + [I]/K_i) + (1 + [I]/\alpha K_i)] \quad (10)$$

$$v = V_{max}[(1 + \beta[I]/\alpha K_i)/(1 + [I]/\alpha K_i)]/[1 + (K_m/[S])(1 + [I]/K_i)/(1 + [I]/\alpha K_i)] \quad (11)$$

K_i represents the equilibrium dissociation constant for the EI (enzyme−inhibitor) complex, and αK_i represents the equilibrium dissociation constant for the ESI complex (enzyme−substrate−inhibitor complex) (Supporting Information 1). For noncompetitive inhibitors, K_i and αK_i are equal ($\alpha = 1$; therefore, $K_i = \alpha K_i$), and eq 10 is simplified to eq 6, giving pure noncompetitive inhibition with the same inhibition degree in the enzyme and the ES complex. If K_i and αK_i are not equal, it becomes a mixed noncompetitive inhibition, with the enzyme−inhibitor binding being dependent on the substrate concentration. The inhibitor also affects the V_{max}; that is to say, the ESI complex is assumed to break down at a velocity different from that of the ES complex, and the rate constants k and k' apply to the breakdown of the ES complex and the EIS complex, respectively (Supporting Information 1). The ESI complex is inactive in complete noncompetitive inhibition ($k' = 0$) (eq 6), but when the inhibitor does break down, though more slowly than ES does [$0 < k'/k(=\beta) < 1$], it becomes partial noncompetitive inhibition (eq 7) (*37*). The selected models can be automatically generated as interactive graphs and then ranked by goodness of fit according to certain fit criteria, including the AIC, R^2, the sum of squares, and the standard error.

All of the kinetic constants and inhibition constants were calculated with the SigmaPlot 9.01 Enzyme Kinetics Module (Systat Software, Inc.). The IC_{50} value was calculated by the four-parameter logistic model with the Levenberg−Marquardt algorithm (No. 205) in XLfit (IDBS, Guildford, U.K.).

Three-Dimensional Model Construction and Docking Simulation. The human WNK1 three-dimensional model with ATP-γ-S was constructed by homology modeling using Modeler (http://salilab.org/modeller/) (*38*). We used rat WNK1 mutant S382A [Protein Data Bank (PDB) entry 1T4H] as the modeling template. Then, we added hydrogen to the model, fixed the main chain, and minimized the molecular energy by the CHARMm22 force field in the molecular operating environment [MOE, Chemical Computing Group, Inc. (http://www.chemcomp.com/)].

The PP1 molecule was constructed by means of Molecular Builder in the MOE software. A docking simulation of human WNK1 with PP1 or ATP-γ-S was conducted using the AutoDock 3.0.5 docking tool (http://autodock.scripps.edu/science). AutoDock is used to perform computational molecular docking of small molecules to proteins and other important macromolecules, by treating the ligand as if it is conformationally flexible (*39*−*41*). AutoDock uses a scoring function based on the AMBER force field and estimates the free energy of the binding of the ligand to its target. To estimate the best docking model for WNK1-PP1, we selected the Lamarckian generic algorithm (LGA) as the search method and then calculated the predicted docking free energies by using the results of 200 runs.

RESULTS

Characterization of the Enzyme in the Caliper Enzyme Assay. The kinetic parameters of the enzyme were determined by using fluorescein-labeled OXSR1 peptide, which is the physiological substrate of WNK1. The K_m values for ATP and the OXSR1 peptide were calculated to be 52.0 ± 0.82 and 68.4 ± 3.71 μM, respectively, in the kinetic mode, by plotting the initial velocity versus the substrate concentration (Supporting Information 2A,B). The specific activity, k_{cat}, was calculated to be $4.56 \pm 0.35\ min^{-1}$. Generally, enzyme reactions are studied under steady state conditions. Therefore, at higher substrate concentrations, the initial velocity appears to reach a maximum level, as if the active site of all the enzyme molecules were saturated with substrate. The averages of the kinetic constants are summarized in Table 1. To evaluate the detection range of the fluorescence detector on Labchip 3000, the fluorescein-labeled substrate peptide was diluted to determine its signal. As shown in Supporting Information 3A, fluorescence levels of up to 60 μM peptide showed linear regression with a correlation coefficient of 0.99. To optimize the assay conditions, the adequate WNK1 concentration was determined by changing the initial rate of 25−100 nM GST-WNK1(1−491) at 25 and 800 μM ATP in real-time kinetic mode. The linear initial rates were observed with enzyme concentrations of up to 80 nM at 25 μM ATP with a correlation coefficient of 0.99 (Supporting Information 3B). For the reaction at 800 μM ATP, the correlation coefficient (0.98) confirmed the linearity up to 60 nM WNK1. The assay was found to have a high linearity in the low concentration range of WNK1.

Initial Kinetic Profile of the Bireactant Phosphorylation Reaction Catalyzed by Human WNK1. The two-substrate profile for WNK1 kinase was determined by utilizing a two-dimensional matrix of various concentrations of ATP and OXSR1 peptide. In general, the kinetic mechanisms of enzymatic reactions with two substrates can be classified into sequential reactions and ping-pong reactions by analyzing the initial rate data in the Lineweaver−Burk plots. Sequential mechanisms will exhibit a converging plot pattern, whereas ping-pong mechanisms will give rise to a family of parallel lines with a constant slope. For WNK1, the initial rates were determined at four fixed concentrations of OXSR1 for five different ATP concentrations (Supporting Information 4A). The same set of plots was also generated at four different concentrations of OXSR1 peptide for five fixed ATP concentrations (Supporting Information 4B). The double-reciprocal plots of $1/v$ versus 1/[ATP] and $1/v$ versus 1/[OXSR1 peptide] displayed converging line patterns (Supporting Information 4C,D). The results from two repeated experiments gave identical intersecting patterns in the reciprocal plots. The equilibrium dissociation constants generated by eq 1 for the ternary complex (K_{ia}) with ATP and the OXSR1 peptide were nearly identical to the corresponding K_m values for each of these substrates (Table 2), indicating noninteracting substrate binding. The lack of interaction between the two substrates suggested a random sequential mechanism as opposed to a required order of substrate binding. Moreover, the analysis of the double-reciprocal Lineweaver−Burk plots of $1/v$ versus 1/[ATP] and $1/v$ versus 1/[OXSR1 peptide] revealed a pattern of lines converging at an intersection left of the y-axis (Supporting Information 4C,D), indicating a sequential kinetic mechanism. If it had been a ping-pong mechanism, it would have generated parallel lines in the Lineweaver−Burk plots. From the analysis done with SigmaPlot, the WNK reaction mode was concluded to be a random bi-bi sequential mechanism (Table 2).

Table 1: Kinetic Constants for WNK1 Kinase[a]

substrate	K_m (μM)	k_{cat} (min^{-1})	K_{ia} (μM)
ATP	52.0 ± 0.82	4.56 ± 0.35	73.4 ± 0.50
OXSR1 peptide	68.4 ± 3.71		75.0 ± 4.23

[a]Each parameter obtained from three separate experiments is shown as the mean ± standard deviation.

Table 2: Best-Fit Model of WNK1 Kinetics[a]

rank by AIC	equation	R^2	AIC	sum of squares	runs test
1	random bi-bi (sequential)	1.00	−2.04	0.89	pass
2	ordered bi-bi (sequential)	0.99	76.9	2.42	fail
3	ping-pong bi-bi (nonsequential)	0.99	88.0	2.79	pass

[a]The SigmaPlot enzyme kinetic module provided three different built-in equations for characterizing different types of reaction mechanisms. Several goodness-of-fit criteria, including the AIC (Akaike's information criterion), were adopted to determine the best model automatically. The parameter values of R^2, AIC, sum of squares, and significance level for the tested runs are summarized.

Assay Stability of the Enzyme Assay. In screening a compound in an enzyme assay, one requires a wide dynamic range of assay signals and low data variation associated with the signal measurements. In general, assay stability is assessed by the Z' factor and the signal-to-background ratio (S/B) (*42*). To assess the screening data variability, we defined the QC criteria according to the previous report, as follows: S/B > 10, CV (coefficient of variation) < 10%, and Z' factor > 0.5. We calculated the average of the high control signal intensity as the WNK1 enzyme in the absence of EDTA. The average of the low control signal intensity was calculated as the WNK1 enzyme in the presence of EDTA. For each assay plate, 16 high and 16 low controls were used for calculating the QC and QA values accumulated over a period of 2 months. The values for the Z' factor of the WNK1 enzyme assay were calculated to be always >0.80, and the CV values were calculated to be lower than 10% in the high controls. Therefore, we concluded that the WNK1 enzyme assay is suitable for the assessment of the compounds.

Determination of IC_{50} Values of Inhibitors. To select the WNK1 inhibitor, we tested 86 of the commercially available inhibitors in the Screen-Well Kinase Inhibitor Library (BIOMOL International). Staurosporine (a commercially available inhibitor that inhibits PKA, PKG, CaMK, tyrosine kinases, and phosphorylase kinase), tyrphostin 47 (EGF receptor kinase inhibitor), PP1 (Src family tyrosine kinase inhibitor), and PP2

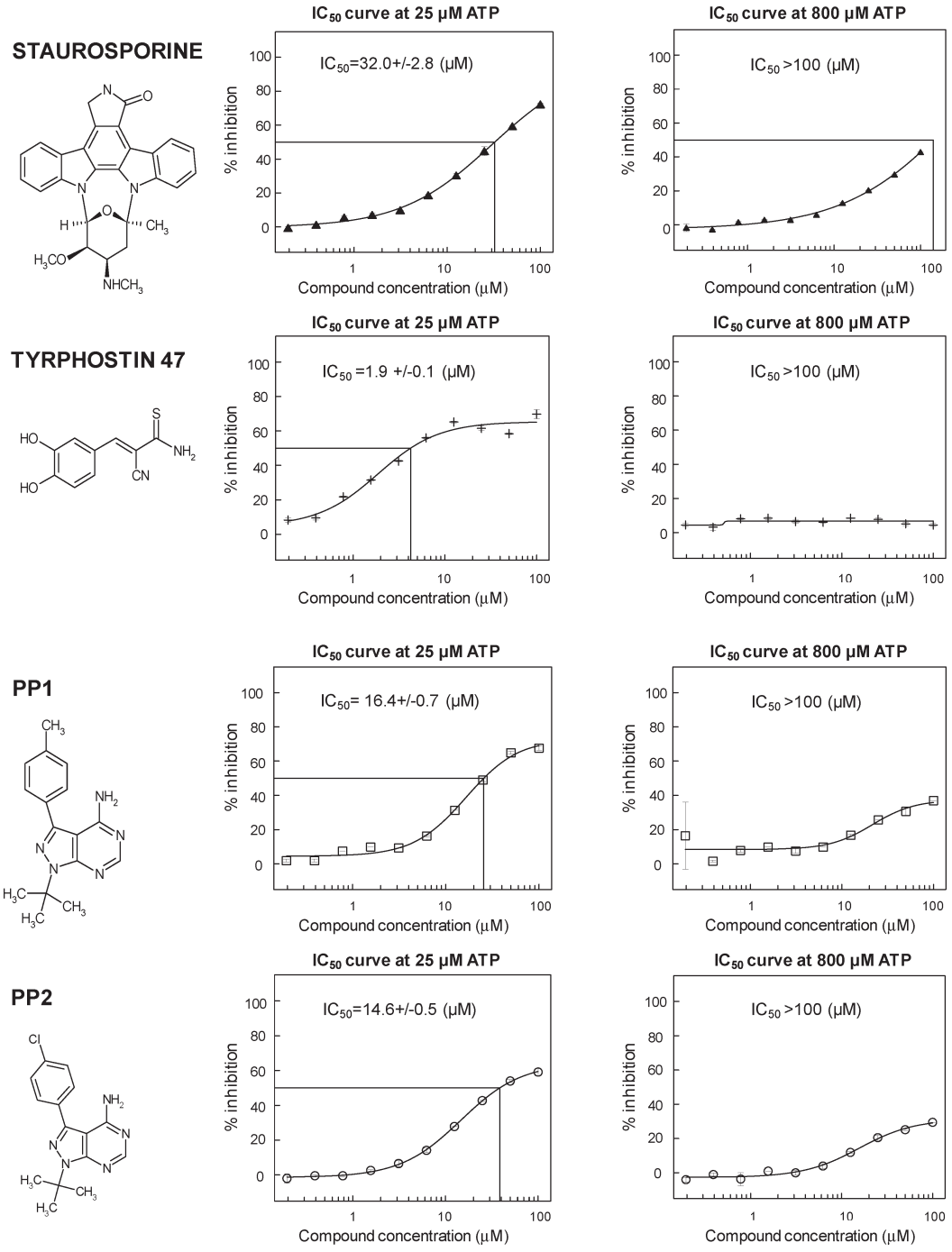

FIGURE 1: IC_{50} curves at a low or a high concentration of ATP. Comparison of the dose-dependent inhibition of the WNK1 activity by four compounds: staurosporine (▲), tyrphostin 47 (+), PP1 (□), and PP2 (○). For the low-ATP reaction, 25 μM ATP and 10 μM OXSR1 peptide were incubated with the dosed compound (from 0.03 to 100 μM) and 25 nM GST-WNK1(1−491) at 25 °C for 3 h. For the high-ATP reaction, 800 μM ATP and 10 μM OXSR1 peptide were incubated with the dosed compound (from 0.03 to 100 μM) and 25 nM GST-WNK1(1−491) at 25 °C for 50 min.

(Src family tyrosine kinase inhibitor) exhibited positive inhibition at 25 μM ATP in the WNK1 mobility shift assay (Figure). Staurosporine exhibited 71% inhibition at the maximum dose without saturation. It might be attributed to the low potency of staurosporine at 100 μM. Because of the DMSO tolerance of the WNK1 enzyme assay, the final concentration of the compound that we could evaluate was 100 μM. Staurosporine might show nearly 100% inhibition at a higher concentration of 100 μM. In fact, the IC_{50} of staurosporine was fitted by the four-parameter logistic model with the maximam percent inhibition being 97% in XLfit, and the Hill coefficient was calculated as 0.9 (data not shown), which indicated that the fitting did not have problem. On the other hand, tyrphostin 47, PP1, and PP2 exhibited approximately 60% incomplete saturated inhibition at the maximal dose because of their low solubility in a 10% DMSO solution (Figure 1). Tyrphostin 47, PP1, and PP2 precipitated from 25 to 100 μM, from 60 to 100 μM, and from 70 to 100 μM, respectively. The IC_{50} values of tyrphostin 47, PP1, and PP2 were fitted by the four-parameter logistic model with the maximal percent inhibition values being 65, 73, and 64%, respectively, in XLfit. The Hill coefficients of these compounds were calculated as 1.3 (data is not shown), which indicated that these compounds

Table 3: Summary of the IC_{50} Values[a] of the Hit Compounds [25 nM GST-WNK1(1−491) and 10 μM OXSR1 peptide]

	Caliper IC_{50} (μM)			
	25 μM ATP		800 μM ATP	
inhibitor	IC_{50} (μM)	compound concentration at 50% inhibition (μM)	IC_{50} (μM)	compound concentration at 50% inhibition (μM)
staurosporine	32.0 ± 2.81	32.4 ± 1.59	> 100	> 100
tyrphostin 47	1.91 ± 0.18	4.23 ± 0.17	> 100	> 100
PP1	16.4 ± 0.72	25.5 ± 0.81	> 100	> 100
PP2	14.6 ± 0.55	38.5 ± 0.74	> 100	> 100
phospho-OXSR1	131 ± 0.91	125 ± 0.78	not determined	not determined
AMP-PNP	127 ± 4.52	112 ± 6.60	270 ± 4.52	285 ± 14.2

[a]The IC_{50} values at the low (25 μM) and high (800 μM) ATP concentrations of the hit compounds were determined by the Caliper enzyme assay. The IC_{50} values from the dose−response curve fitting and the compound concentrations at the 50% inhibition point are listed. An ideally fitting IC_{50} corresponds to a 50% inhibition concentration.

Table 4: Inhibition Constants and Modes of Action for WNK1 Kinase[a]

inhibitor	variable substrate	inhibition mode of action (MOA)	K_i (μM)	αK_i (μM)
staurosporine	ATP	mixed (partial)	16.4 ± 0.57	110 ± 0.55
	OXSR1 peptide	noncompetitive (partial)	61.2 ± 4.74	61.2 ± 4.74
tyrphostin 47	ATP	competitive (partial)	11.8 ± 1.04	not determined
	OXSR1 peptide	not determined	not determined	not determined
PP1	ATP	competitive (partial)	12.7 ± 1.49	not determined
	OXSR1 peptide	noncompetitive (partial)	48.5 ± 3.79	48.5 ± 3.79
PP2	ATP	mixed (partial)	13.3 ± 0.85	59.7 ± 3.79
	OXSR1 peptide	mixed (full)	47.5 ± 3.95	94.1 ± 0.46
phospho-OXSR1	ATP	noncompetitive (partial)	191 ± 39.1	191 ± 39.1
	OXSR1 peptide	mixed (partial)	86.7 ± 10.6	225 ± 0.31
AMP-PNP	ATP	competitive (full)	44.7 ± 5.96	not determined
	OXSR1 peptide	not determined	not determined	not determined

[a]The inhibition constants were calculated using the equation in SigmaPlot. The errors shown are standard errors. The data are from a single experiment performed in triplicate. The αK_i values were calculated as points of x-axis intersection of the secondary plots of the intercepts ($1/V_{max}$) from the Lineweaver−Burk plots (y-axis) via the inhibitor concentration (x-axis).

have solubility limitations. This could be important information for setting the range of compound concentrations without precipitation for analyzing the inhibitor's mode of action (MOA).

To confirm the validity of the WNK1 mobility shift assay, we calculated the IC_{50} value of the hit compound in the commercially available FP-based WNK1 IMAP assay. We confirmed that the potency of the hit compounds in the WNK1 mobility shift assay correlated well with the results of the FP-based WNK1 IMAP assay (Supporting Information 5). Because the IMAP assay has an upper limit on the ATP concentration, the WNK1 mobility shift assay was used for further investigation of the inhibitor mode of action.

To distinguish the ATP competitive inhibitor and ATP non/uncompetitive inhibitor, the IC_{50} values of the hit compounds were determined at 25 μM ATP (low ATP) and 800 μM ATP (high ATP) in the WNK1 mobility shift assay (Figure 1 and Table 3). The ATP analogue adenosine 5′-(β,γ-imido)triphosphate tetralithium salt hydrate (AMP-PNP) and phospho-OXSR1 peptide were tested in the same assay as controls. The ATP analogue AMP-PNP exhibited a > 2-fold shift in the IC_{50} between the high and low ATP concentrations in the same assay. The peptide competitor phospho-OXSR1 peptide exhibited a potency similar to that of AMP-PNP. All of the hit compounds exhibited micromolar potency in the WNK1 Caliper enzyme assay and a > 3-fold shift in the IC_{50} between the high and low ATP concentrations, like AMP-PNP (Table 3). This indicates that the hit compounds might all be ATP competitors.

MOA Analysis of the Hit Compounds. To extend the results of the IC_{50} shift between the low and high ATP concentrations, we investigated the mechanism of WNK1 inhibition for the hit compounds. The inhibition constant versus ATP and OXSR1 was calculated by means of the SigmaPlot Enzyme Kinetics Module. The results of the analysis of the inhibitor's mode of action (MOA) are summarized in Table 4.

The best fit inhibition mode for staurosporine at various ATP concentrations was found to be mixed-type inhibition by SigmaPlot analysis. However, the Lineweaver−Burk plots (Figure 2A) intersected near the y-axis with ATP, and the αK_i value was calculated to be 6 times higher than the K_i value. These results indicate that the affinity of the EI (enzyme−inhibitor) complex is much tighter than that of the ESI (enzyme−substrate−inhibitor) complex. Therefore, we conclude that staurosporine is a mixed-type inhibitor against ATP which is near-competitive inhibition. As for the inhibition mode against the OXSR1 peptide substrate, staurosporine inhibited the enzyme activity in a noncompetitive manner at various OXSR1 peptide concentrations (Figure 2B).

The inhibition mode of PP1 was calculated to be ATP-competitive (partial) inhibition. As shown in Figure 2C, when ATP was set as the variable substrate, the Lineweaver−Burk plots for several fixed inhibitor concentrations of PP1 exhibited a common intercept on the y-axis with slopes increasing linearly with inhibitor concentration. When the OXSR1 peptide concentration was varied in the presence of various concentrations of PP1, the Lineweaver−Burk plots generated a noncompetitive

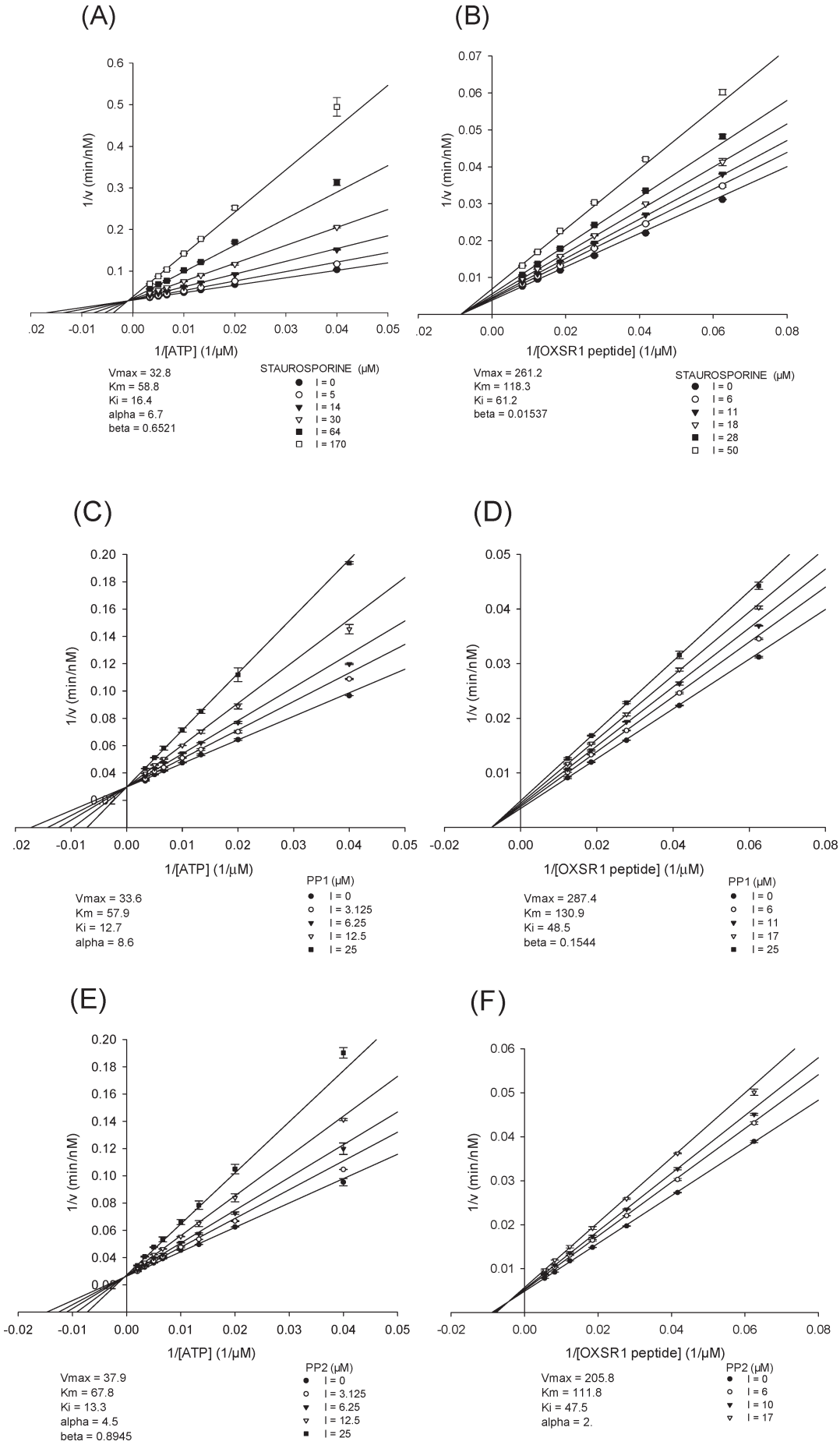
(A)
1/v (min/nM)
1/[ATP] (1/μM)
Vmax = 32.8
Km = 58.8
Ki = 16.4
alpha = 6.7
beta = 0.6521
STAUROSPORINE (μM)
I = 0
I = 5
I = 14
I = 30
I = 64
I = 170
(B)
1/v (min/nM)
1/[OXSR1 peptide] (1/μM)
Vmax = 261.2
Km = 118.3
Ki = 61.2
beta = 0.01537
STAUROSPORINE (μM)
I = 0
I = 6
I = 11
I = 18
I = 28
I = 50
(C)
1/v (min/nM)
1/[ATP] (1/μM)
Vmax = 33.6
Km = 57.9
Ki = 12.7
alpha = 8.6
PP1 (μM)
I = 0
I = 3.125
I = 6.25
I = 12.5
I = 25
(D)
1/v (min/nM)
1/[OXSR1 peptide] (1/μM)
Vmax = 287.4
Km = 130.9
Ki = 48.5
beta = 0.1544
PP1 (μM)
I = 0
I = 6
I = 11
I = 17
I = 25
(E)
1/v (min/nM)
1/[ATP] (1/μM)
Vmax = 37.9
Km = 67.8
Ki = 13.3
alpha = 4.5
beta = 0.8945
PP2 (μM)
I = 0
I = 3.125
I = 6.25
I = 12.5
I = 25
(F)
1/v (min/nM)
1/[OXSR1 peptide] (1/μM)
Vmax = 205.8
Km = 111.8
Ki = 47.5
alpha = 2.
PP2 (μM)
I = 0
I = 6
I = 10
I = 17

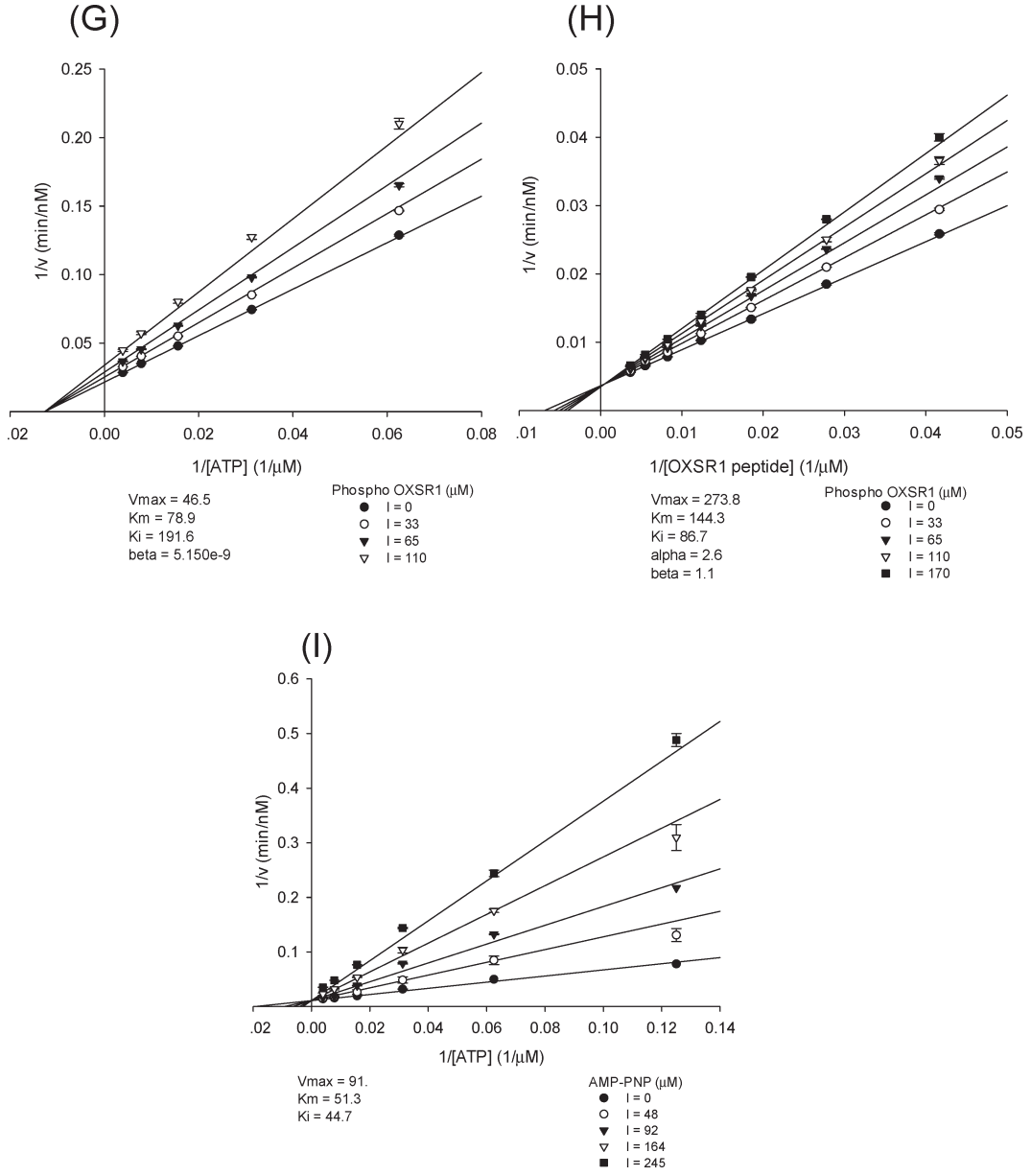

FIGURE 2: Analysis of the inhibition mechanism of compound inhibition with ATP and the OXSR1 peptide as the variable substrates. (A) Lineweaver−Burk plot of $1/v$ (min/nM) vs 1/[ATP] (μM^{-1}) at six fixed staurosporine concentrations. GST-WNK1 and the OXSR1 peptide were fixed at concentrations of 10 μM and 25 nM, respectively. The ATP concentration was varied from 4 to 512 μM. The enzyme reaction was performed at 25 °C for 50 min. (B) Lineweaver−Burk plot of $1/v$ (min/nM) vs 1/[OXSR1 peptide] (μM^{-1}) at six fixed staurosporine concentrations. The OXSR1 peptide concentration was varied from 16 to 273 μM. (C) Double-reciprocal plot of $1/v$ (min/nM) vs 1/[ATP] (μM^{-1}) at five fixed PP1 concentrations. (D) Double-reciprocal plot of $1/v$ (min/nM) vs 1/[OXSR1 peptide] (μM^{-1}) at five fixed PP1 concentrations. (E) Double-reciprocal plot of $1/v$ (min/nM) vs 1/[ATP] (μM^{-1}) at five fixed PP2 concentrations. (F) Double-reciprocal plot of $1/v$ (min/nM) vs 1/[OXSR1 peptide] (μM^{-1}) at four fixed PP2 concentrations. (G) Double-reciprocal plot of $1/v$ (min/nM) vs 1/[ATP] (μM^{-1}) at four fixed p-OXSR1 concentrations. The sequence of p-OXSR1 is RVPGSpSGRLHK: the amino acid sequence of residues 320−330 in human OXSR1. (H) Double-reciprocal plot of $1/v$ (min/nM) vs 1/[OXSR1 peptide] (μM^{-1}) at five fixed p-OXSR1 concentrations. (I) Double-reciprocal plot of $1/v$ (min/nM) vs 1/[ATP] (μM^{-1}) at five fixed AMP-PNP concentrations.

inhibition pattern (Figure 2D). We concluded that PP1 was competitive against ATP, with a K_i value of 12.7 μM, and noncompetitive against the OXSR1 peptide, with a K_i value of 48.5 μM.

PP2 was calculated to be a mixed inhibitor of ATP and OXSR1 peptide with SigmaPlot (Table 4). The plot pattern against ATP was close to that typical of competitive inhibition (Figure 2E), and the αK_i value was calculated to be 4 times higher than the K_i value. On the other hand, the αK_i value for the OXSR1 peptide was calculated to be 2 times higher than the K_i value (Figure 2F and Table 4). This indicates that PP2 preferentially binds to the free enzyme.

To validate the MOA analysis, we chose the phosphorylated OXSR1 peptide (p-OXSR1), which contained a phospho-acceptor site, and an ATP mimic, AMP-PNP, as the peptide and ATP competitive control, respectively. The phospho-peptide exhibited noncompetitive inhibition against ATP in the same assay and mixed inhibition against the OXSR1 peptide (Figure 2G,H). AMP-PNP exhibited a pattern typical of ATP competitors, in that the double-reciprocal plots of the velocity versus concentration showed intersecting lines at the y-axis versus ATP (Figure 2I) as well as PP1. These results of the inhibition mode were consistent with the random sequential mechanism with

noninteracting substrate-binding sites in the random bi-bi sequential mechanism determined by our calculations and are listed in Table 2.

DISCUSSION

Kinetic Mechanism. In this study, we determined the kinetic mechanism for WNK1 kinase with two substrates, ATP and the OXSR1 peptide. From the initial rate data analysis based on the Lineweaver−Burk plots, the kinetic mechanism of WNK kinase was found to be a random bi-bi sequential mechanism. Generally, enzymatic reactions with two substrates can be separated into two major categories: sequential reactions and ping-pong reactions (*43*). Sequential mechanisms exhibit a converging plot pattern (noncompetitive inhibition pattern), whereas ping-pong mechanisms give several parallel lines with a constant slope (uncompetitive inhibition pattern). As for WNK1, ATP and the OXSR1 peptide exhibited a noncompetitive inhibition pattern against each substrate (Supporting Information 3). This indicates that WNK1 might randomly bind ATP and OXSR1 peptide to form a ternary complex. The initial velocity data also showed no disparity between the K_m and the K_{ia} for either substrate (Table 1), also suggesting noninteracting substrate binding. This basic understanding of the kinetic characteristics of WNK1 enables us to design not only ATP-competitive inhibitors but also specific peptide-competitive inhibitors.

Determination of IC_{50} Values and MOA Analysis of the WNK1 Inhibitor. This is the first report of a chip-based microfluidic WNK1 enzymatic assay, and of the discovery of a WNK1 inhibitor from a commercially available library. The Caliper mobility shift assay technology is a chip-based microfluidic method. Differently charged substrate peptides and products have different migration rates in the electronic field on the chip. Substrates and products are quantitatively determined on the basis of fluorescence signal ratiometry. Because this assay imposes no upper limit on the ATP concentration, we were able to determine the IC_{50} value at various concentrations of ATP, from the K_m value to the $32K_m$ value. In general, the ATP competitor shows a >3-fold shift of the IC_{50} value at the high ATP concentration; therefore, it is easy to distinguish the ATP competitor from the noncompetitor. Utilizing the OXSR1 peptide, the physiological substrate of WNK1, we are able to detect the WNK1 activity, provided that it is in the immediate vicinity within the cell. It is known that the wild-type WNK1 kinase domain becomes autophosphorylated, acquiring the active conformation when expressed in both *Escherichia coli* and insect cells (*22*). Therefore, peptide-competitive inhibitors or allosteric inhibitors that recognize the active conformation of WNK1 will detect WNK1 in this assay. The robustness of our novel WNK1 enzymatic assay was confirmed, in that all assay plates revealed Z' factor values of >0.80. By utilizing the hit compound, we validated the stability and reproducibility of the IC_{50} determination protocol of the WNK1 enzyme assay.

We further investigated the mode of action (MOA) of the hit inhibitor. Utilizing AMP-PNP (ATP analogue) and the phospho-OXSR1 peptide, we verified the MOA analysis using SigmaPlot. The hit compounds of WNK1, i.e., staurosporine and PP1, exhibited the same inhibition mode as AMP-PNP, indicating that these compounds were near ATP competitors. In addition, staurosporine and PP1 exhibited noncompetitive inhibition against the OXSR1 peptide, suggesting that there is no substantial cooperative interaction between the ATP site and the OXSR1 peptide docking site on WNK1. This finding is fully consistent with the kinetic mechanism of WNK1, which is a random bi-bi sequential mechanism.

It was interesting that only Src family kinases (Hck, Lck, and Src) and EGFR inhibitors exhibited positive inhibition against WNK1, since WNK1 is a Ser-Thr kinase. PP1 (Src family kinase inhibitors) and tyrphostin 47 (EGFR inhibitor) inhibited WNK1 in the ATP-competitive mode. Although the kinase domains of Hck, Lck, Src, and WNK1 have low degrees of amino acid sequence identity (26.5, 28.0, and 26.3%, respectively), the kinase domain structures resemble WNK1 closely, having root-mean-square deviations of 2.3, 1.1, and 1.0 Å, respectively. It is not rare for one kinase inhibitor to show a similar effect against kinases with a low degree of sequence identity ($<50\%$) (*44*). Recently, the classification of kinases based on small-molecule selectivity data instead of sequence-based clustering has been reported as a new approach to drug discovery (*44*−*46*). To clarify the reason why the Src family kinase inhibitor inhibited WNK1, we compared WNK1 with the Src family kinase, Hck, from the structural point of view. To compare the mode of binding of PP1 with Hck and WNK1, we constructed a three-dimensional model of the human WNK1 kinase domain docked with PP1 (Figure 3A). The structure of the Hck−PP1 complex (PDB entry 1QCF) was reported in 1999. In the Hck−PP1 complex, PP1 is indeed bound within the nucleotide-binding pocket, in which it occupies the site where the adenine base is normally bound (*47*). The structure of PP1 resembles, in part, that of the purine ring of ATP, and the analysis of the kinetic data suggests that its binding to Src kinases is competitive with ATP (*48*). The amino group of PP1 in Hck is hydrogen-bonded to the side chain hydroxyl of Thr333 (Thr338 in PDB entry 1QCF) and the main chain carbonyl of Glu334 (Glu338 in PDB entry 1QCF). The nitrogen at position 3 accepts a hydrogen bond from the main chain amide of Met336 (Met341 in PDBentry 1QCF), and the nitrogen at position 6 interacts with Lys290 (Lys295 in PDB entry 1QCF) via a well-ordered water molecule (*47*). The IC_{50} values for the inhibition of the catalytic activity by PP1 range from 5 to 170 nM for the Src family tyrosine kinases, whereas PP1 is less active against WNK1 and inactive against PKA, ZAP-70, and Jak2 (*48*). As in PKA, the position corresponding to Thr333 in Hck is occupied by methionine in ZAP70 and Jak2 (Figure 4). This indicates that Thr333 is a major residue in the interaction with PP1.

From the docking results of WNK1 and PP1, it is clear that the position of PP1 partially overlapped that of Hck, and the hydrogen bond interaction of PP1 with Thr, Glu, and Met was well-conserved (Figure 3A). In particular, the pyrazolopyrimidine rings of PP1 bound to WNK1 were positioned via a hydrogen bond interaction with Thr301 (Thr333 in Hck), Glu302 (Glu334 in Hck), and Met304 (Met336 in Hck) (Figure 3A,B). Generally, the Thr333 in Hck is called a "gatekeeper", which is a residue structurally identified to be one of the major determinants of selectivity in kinases. Twenty percent of kinases have Thr and 40% Met in the gatekeeper position. Remarkably, 90% of tyrosine kinases have Thr in this position. In WNK1, Thr301 corresponds to the gatekeeper. We found that, since WNK1 is classified as a Ser-Thr kinase, it has the same species of gatekeeper as all tyrosine kinases. The difference in hydrophobic packing between Src family members EGFR and WNK1 is discussed in Supporting Information 6.

We finally confirmed the difference in the catalytic site in WNK1 and Hck by constructing a three-dimensional model of the WNK1-ATP-γ-S complex using AutoDock and then

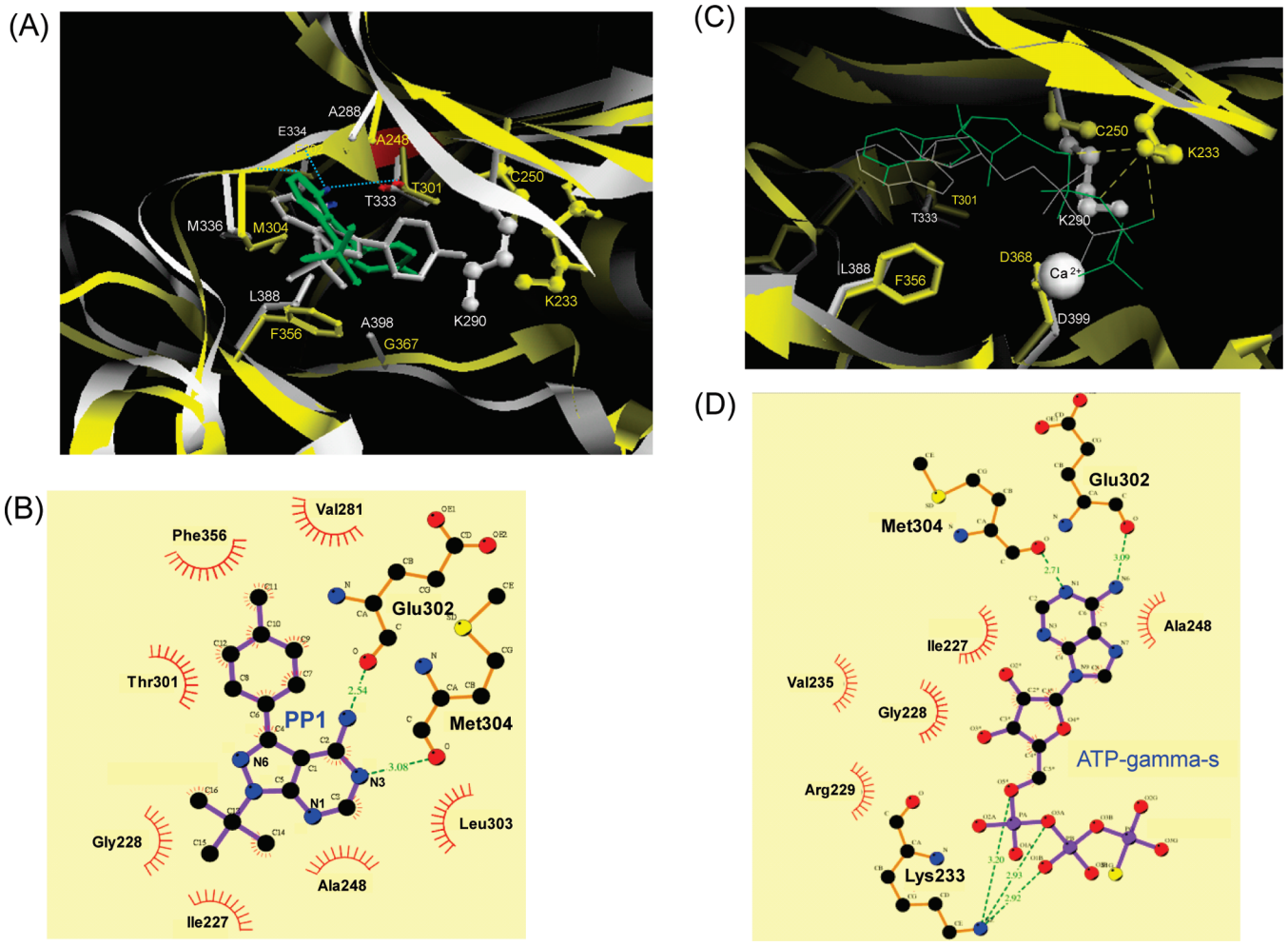

FIGURE 3: Comparison of the active sites of WNK1 and Hck with PP1, an ATP analogue. (A) Superposition of human WNK1 (yellow) with PP1 (green) and Hck (1QCF) with PP1 (*49*). Hydrogen bond interactions are depicted as dashed lines. (B) Hydrogen bond interaction of the active site in the WNK1 residue with PP1. (C) Superposition of human WNK1 (yellow) with ATP-γ-S (green) and Hck (1AD5) (*49*) with AMP-PNP (adenylyl imidodiphosphate tetralithium salt) (*49*). Hydrogen bond interactions are depicted as dashed lines. (D) Hydrogen bond interaction of the active site in the WNK1 residue with ATP-γ-S.

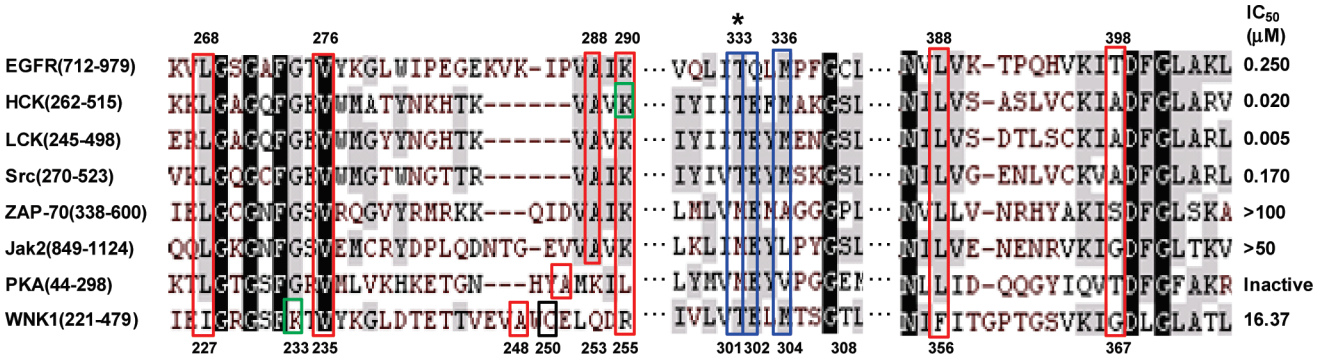

FIGURE 4: Sequence comparison of the Src kinase family members and PKA with WNK1. The inhibition constants (IC_{50}) for PP1 were taken from ref *50*. The catalytic Lys290 in Hck and Lys233 in WNK1 are enclosed in green boxes. The residues hydrogen-bonded with PP1 are enclosed in blue boxes. The hydrophobic residues interacting with PP1 are enclosed in red boxes.

overlaying it with the model for the Hck−AMP-PNP complex (Figure 3C). It is well-known that WNK1 has a unique catalytic site (*22*). The catalytic lysine residue, Lys290, in Hck is replaced with Cys250 in WNK1, which induces the formation of a large cavity and a unique active site. The Src family kinases (Hck, Lck, and Src) and EGFR do not have a Cys residue in the catalytic site. Cys250 in WNK1 is far from the active site and is therefore not likely to be a candidate for catalysis. The lysine residue (Lys233) next to Cys250 in WNK1 reaches into the active site and makes a hydrogen bond with the phosphate group (Figure 3C). Furthermore, the binding position of ATP-γ-S overlaps with that of AMP-PNP in Hck (Figure 3C). The pyrazolopyrimidine rings of ATP-γ-S are constructed through a hydrogen bond interaction with the hinge region of Met304 and Glu302 in WNK1 (Figure 3C) as well as the PP1−WNK1 complex. This indicates that it is difficult to design a specific WNK1 inhibitor by using the

hinge region, but by filling the space around Cys250, we might be able to design a specific WNK1 inhibitor that does not inhibit the Src family kinases and EGFR.

In this study, we found that the kinetic mechanism for WNK1 is randomly sequential for ATP and the OXSR1 peptide. Among the WNK1 inhibitors selected from commercially available inhibitors, only Src family kinases (Hck, Lck, and Src) and EGFR inhibitors exhibited positive inhibition at an IC_{50} value in the micromolar range in the enzyme assay. By understanding small molecules and targets, we can find unpredictable related kinases for WNK1. In the future, a combination of high-quality test compounds, assay technology, enzyme kinetics, structural biology, and cell assays will enable us to identify specific kinase inhibitors for use in the treatment of hypertension and related diseases.

ACKNOWLEDGMENT

We thank Mr. Fumikazu Goto for his helpful assistance in the construction of our novel assay.

SUPPORTING INFORMATION AVAILABLE

Additional experimental observations. This material is available free of charge via the Internet at http://pubs.acs.org.

REFERENCES

1. Gordon, R. K., Sr., Tunny, T., and Stowasser, M. (1995) Hypertension: Pathophysiology, Diagnosis, and Management (Laragh, J. H., and Brenner, B. M., Eds.) pp 2111−2123, Raven, New York.
2. Mayan, H., Vered, I., Mouallem, M., Tzadok-Witkon, M., Pauzner, R., and Farfel, Z. (2002) Pseudohypoaldosteronism type II: Marked sensitivity to thiazides, hypercalciuria, normomagnesemia, and low bone mineral density. *J. Clin. Endocrinol. Metab. 87*, 3248–3254.
3. Verissimo, F., and Jordan, P. (2001) WNK kinases, a novel protein kinase subfamily in multi-cellular organisms. *Oncogene 20*, 5562–5569.
4. Wilson, F. H., Disse-Nicodeme, S., Choate, K. A., Ishikawa, K., Nelson-Williams, C., Desitter, I., Gunel, M., Milford, D. V., Lipkin, G. W., Achard, J. M., Feely, M. P., Dussol, B., Berland, Y., Unwin, R. J., Mayan, H., Simon, D. B., Farfel, Z., Jeunemaitre, X., and Lifton, R. P. (2001) Human hypertension caused by mutations in WNK kinases. *Science 293*, 1107–1112.
5. Zambrowicz, B. P., Abuin, A., Ramirez-Solis, R., Richter, L. J., Piggott, J., BeltrandelRio, H., Buxton, E. C., Edwards, J., Finch, R. A., Friddle, C. J., Gupta, A., Hansen, G., Hu, Y., Huang, W., Jaing, C., Key, B. W.Jr., Kipp, P., Kohlhauff, B., Ma, Z. Q., Markesich, D., Payne, R., Potter, D. G., Qian, N., Shaw, J., Schrick, J., Shi, Z. Z., Sparks, M. J., Van Sligtenhorst, I., Vogel, P., Walke, W., Xu, N., Zhu, Q., Person, C., and Sands, A. T. (2003) Wnk1 kinase deficiency lowers blood pressure in mice: A gene-trap screen to identify potential targets for therapeutic intervention. *Proc. Natl. Acad. Sci. U.S.A. 100*, 14109–14114.
6. Lalioti, M. D., Zhang, J., Volkman, H. M., Kahle, K. T., Hoffmann, K. E., Toka, H. R., Nelson-Williams, C., Ellison, D. H., Flavell, R., Booth, C. J., Lu, Y., Geller, D. S., and Lifton, R. P. (2006) Wnk4 controls blood pressure and potassium homeostasis via regulation of mass and activity of the distal convoluted tubule. *Nat. Genet. 38*, 1124–1132.
7. Yang, S. S., Morimoto, T., Rai, T., Chiga, M., Sohara, E., Ohno, M., Uchida, K., Lin, S. H., Moriguchi, T., Shibuya, H., Kondo, Y., Sasaki, S., and Uchida, S. (2007) Molecular pathogenesis of pseudohypoaldosteronism type II: Generation and analysis of a Wnk4-(D561A/+) knockin mouse model. *Cell Metab. 5*, 331–344.
8. Anselmo, A. N., Earnest, S., Chen, W., Juang, Y. C., Kim, S. C., Zhao, Y., and Cobb, M. H. (2006) WNK1 and OSR1 regulate the Na^+, K^+, $2Cl^-$ cotransporter in HeLa cells. *Proc. Natl. Acad. Sci. U.S.A. 103*, 10883–10888.
9. Richardson, C., Rafiqi, F. H., Karlsson, H. K., Moleleki, N., Vandewalle, A., Campbell, D. G., Morrice, N. A., and Alessi, D. R. (2008) Activation of the thiazide-sensitive Na^+-Cl^- cotransporter by the WNK-regulated kinases SPAK and OSR1. *J. Cell Sci. 121*, 675–684.
10. Piechotta, K., Garbarini, N., England, R., and Delpire, E. (2003) Characterization of the interaction of the stress kinase SPAK with the Na^+-K^+-$2Cl^-$ cotransporter in the nervous system: Evidence for a scaffolding role of the kinase. *J. Biol. Chem. 278*, 52848–52856.
11. Vitari, A. C., Deak, M., Morrice, N. A., and Alessi, D. R. (2005) The WNK1 and WNK4 protein kinases that are mutated in Gordon's hypertension syndrome phosphorylate and activate SPAK and OSR1 protein kinases. *Biochem. J. 391*, 17–24.
12. Gagnon, K. B., England, R., and Delpire, E. (2006) Volume sensitivity of cation-Cl^- cotransporters is modulated by the interaction of two kinases: Ste20-related proline-alanine-rich kinase and WNK4. *Am. J. Physiol. 290*, 134–142.
13. Piechotta, K., Lu, J., and Delpire, E. (2002) Cation chloride cotransporters interact with the stress-related kinases Ste20-related proline-alanine-rich kinase (SPAK) and oxidative stress response 1 (OSR1). *J. Biol. Chem. 277*, 50812–50819.
14. Moriguchi, T., Urushiyama, S., Hisamoto, N., Iemura, S., Uchida, S., Natsume, T., Matsumoto, K., and Shibuya, H. (2005) WNK1 regulates phosphorylation of cation-chloride-coupled cotransporters via the STE20-related kinases, SPAK and OSR1. *J. Biol. Chem. 280*, 42685–42693.
15. Vitari, A. C., Thastrup, J., Rafiqi, F. H., Deak, M., Morrice, N. A., Karlsson, H. K., and Alessi, D. R. (2006) Functional interactions of the SPAK/OSR1 kinases with their upstream activator WNK1 and downstream substrate NKCC1. *Biochem. J. 397*, 223–231.
16. Dowd, B. F., and Forbush, B. (2003) PASK (proline-alanine-rich STE20-related kinase), a regulatory kinase of the Na-K-Cl cotransporter (NKCC1). *J. Biol. Chem. 278*, 27347–27353.
17. Zagorska, A., Pozo-Guisado, E., Boudeau, J., Vitari, A. C., Rafiqi, F. H., Thastrup, J., Deak, M., Campbell, D. G., Morrice, N. A., Prescott, A. R., and Alessi, D. R. (2007) Regulation of activity and localization of the WNK1 protein kinase by hyperosmotic stress. *J. Cell Biol. 176*, 89–100.
18. Xu, B., English, J. M., Wilsbacher, J. L., Stippec, S., Goldsmith, E. J., and Cobb, M. H. (2000) WNK1, a novel mammalian serine/threonine protein kinase lacking the catalytic lysine in subdomain II. *J. Biol. Chem. 275*, 16795–16801.
19. Xu, B. E., Lee, B. H., Min, X., Lenertz, L., Heise, C. J., Stippec, S., Goldsmith, E. J., and Cobb, M. H. (2005) WNK1: Analysis of protein kinase structure, downstream targets, and potential roles in hypertension. *Cell Res. 15*, 6–10.
20. Xu, B. E., Min, X., Stippec, S., Lee, B. H., Goldsmith, E. J., and Cobb, M. H. (2002) Regulation of WNK1 by an autoinhibitory domain and autophosphorylation. *J. Biol. Chem. 277*, 48456–48462.
21. Villa, F., Goebel, J., Rafiqi, F. H., Deak, M., Thastrup, J., Alessi, D. R., and van Aalten, D. M. (2007) Structural insights into the recognition of substrates and activators by the OSR1 kinase. *EMBO Rep. 8*, 839–845.
22. Min, X., Lee, B. H., Cobb, M. H., and Goldsmith, E. J. (2004) Crystal structure of the kinase domain of WNK1, a kinase that causes a hereditary form of hypertension. *Structure 12*, 1303–1311.
23. Niu, L., Chang, K. C., Wilson, S., Tran, P., Zuo, F., and Swinney, D. C. (2007) Kinetic characterization of human JNK2α2 reaction mechanism using substrate competitive inhibitors. *Biochemistry 46*, 4775–4784.
24. Ember, B., Kamenecka, T., and LoGrasso, P. (2008) Kinetic mechanism and inhibitor characterization for c-jun-N-terminal kinase 3α1. *Biochemistry 47*, 3076–3084.
25. Glickman, J. F., Schmid, A., and Ferrand, S. (2008) Scintillation proximity assays in high-throughput screening. *Assay Drug Dev. Technol. 6*, 433–455.
26. Park, Y. W., Cummings, R. T., Wu, L., Zheng, S., Cameron, P. M., Woods, A., Zaller, D. M., Marcy, A. I., and Hermes, J. D. (1999) Homogeneous proximity tyrosine kinase assays: Scintillation proximity assay versus homogeneous time-resolved fluorescence. *Anal. Biochem. 269*, 94–104.
27. Olive, D. M. (2004) Quantitative methods for the analysis of protein phosphorylation in drug development. *Expert Rev. Proteomics 1*, 327–341.
28. Sportsman, J. R., Gaudet, E. A., and Boge, A. (2004) Immobilized metal ion affinity-based fluorescence polarization (IMAP): Advances in kinase screening. *Assay Drug Dev. Technol. 2*, 205–214.
29. Suresh Babu, C. V., Cho, S. G., and Yoo, Y. S. (2005) Method development and measurements of endogenous serine/threonine Akt phosphorylation using capillary electrophoresis for systems biology. *Electrophoresis 26*, 3765–3772.
30. Rowe, T., Hale, C., Zhou, A., Kurzeja, R. J., Ali, A., Menjares, A., Wang, M., and McCarter, J. D. (2006) A high-throughput

microfluidic assay for SH2 domain-containing inositol 5-phosphatase 2. *Assay Drug Dev. Technol. 4*, 175–183.
31. Macarron, R., Mensah, L., Cid, C., Carranza, C., Benson, N., Pope, A. J., and Diez, E. (2000) A homogeneous method to measure aminoacyl-tRNA synthetase aminoacylation activity using scintillation proximity assay technology. *Anal. Biochem. 284*, 183–190.
32. Loomans, E. E., van Doornmalen, A. M., Wat, J. W., and Zaman, G. J. (2003) High-throughput screening with immobilized metal ion affinity-based fluorescence polarization detection, a homogeneous assay for protein kinases. *Assay Drug Dev. Technol. 1*, 445–453.
33. Turek-Etienne, T. C., Kober, T. P., Stafford, J. M., and Bryant, R. W. (2003) Development of a fluorescence polarization AKT serine/threonine kinase assay using an immobilized metal ion affinity-based technology. *Assay Drug Dev. Technol. 1*, 545–553.
34. Cohen, C. B., Chin-Dixon, E., Jeong, S., and Nikiforov, T. T. (1999) A microchip-based enzyme assay for protein kinase A. *Anal. Biochem. 273*, 89–97.
35. Lin, S., Fischl, A. S., Bi, X., and Parce, W. (2003) Separation of phospholipids in microfluidic chip device: Application to high-throughput screening assays for lipid-modifying enzymes. *Anal. Biochem. 314*, 97–107.
36. Shapiro, A., Rivin, O., Gao, N., and Hajec, L. (2005) A homogeneous, high-throughput fluorescence resonance energy transfer-based DNA polymerase assay. *Anal. Biochem. 347*, 254–261.
37. Yoshino, M. (1987) A graphical method for determining inhibition parameters for partial and complete inhibitors. *Biochem. J. 248*, 815–820.
38. Sali, A., and Blundell, T. L. (1993) Comparative protein modelling by satisfaction of spatial restraints. *J. Mol. Biol. 234*, 779–815.
39. Goodsell, D. S., and Olson, A. J. (1990) Automated docking of substrates to proteins by simulated annealing. *Proteins 8*, 195–202.
40. Morris, G. M., Goodsell, D. S., Huey, R., and Olson, A. J. (1996) Distributed automated docking of flexible ligands to proteins: parallel applications of AutoDock 2.4. *J. Comput.-Aided Mol. Des. 10*, 293–304.
41. Morris, G. M., Goodsell, D. S., Halliday, R. S., Huey, R., Hart, W. E., Belew, R. K., and Olson, A. J. (1998) Automated docking using Lamarckian genetic algorithm and an empirical binding free energy function. *J. Comput. Chem. 19*, 1639–1662.
42. Zhang, J. H., Chung, T. D., and Oldenburg, K. R. (1999) A Simple Statistical Parameter for Use in Evaluation and Validation of High Throughput Screening Assays. *J. Biomol. Screening 4*, 67–73.
43. Cleland, W. W. (1963) The kinetics of enzyme-catalyzed reactions with two or more substrates or products. III. Prediction of initial velocity and inhibition patterns by inspection. *Biochim. Biophys. Acta 67*, 188–196.
44. Vieth, M., Higgs, R. E., Robertson, D. H., Shapiro, M., Gragg, E. A., and Hemmerle, H. (2004) Kinomics-structural biology and chemogenomics of kinase inhibitors and targets. *Biochim. Biophys. Acta 1697*, 243–257.
45. Bamborough, P., Drewry, D., Harper, G., Smith, G. K., and Schneider, K. (2008) Assessment of chemical coverage of kinome space and its implications for kinase drug discovery. *J. Med. Chem. 51*, 7898–7914.
46. Karaman, M. W., Herrgard, S., Treiber, D. K., Gallant, P., Atteridge, C. E., Campbell, B. T., Chan, K. W., Ciceri, P., Davis, M. I., Edeen, P. T., Faraoni, R., Floyd, M., Hunt, J. P., Lockhart, D. J., Milanov, Z. V., Morrison, M. J., Pallares, G., Patel, H. K., Pritchard, S., Wodicka, L. M., and Zarrinkar, P. P. (2008) A quantitative analysis of kinase inhibitor selectivity. *Nat. Biotechnol. 26*, 127–132.
47. Schindler, T., Sicheri, F., Pico, A., Gazit, A., Levitzki, A., and Kuriyan, J. (1999) Crystal structure of Hck in complex with a Src family-selective tyrosine kinase inhibitor. *Mol. Cell 3*, 639–648.
48. Hanke, J. H., Gardner, J. P., Dow, R. L., Changelian, P. S., Brissette, W. H., Weringer, E. J., Pollok, B. A., and Connelly, P. A. (1996) Discovery of a novel, potent, and Src family-selective tyrosine kinase inhibitor. Study of Lck- and FynT-dependent T cell activation. *J. Biol. Chem. 271*, 695–701.
49. Adrian, F. J., Ding, Q., Sim, T., Velentza, A., Sloan, C., Liu, Y., Zhang, G., Hur, W., Ding, S., Manley, P., Mestan, J., Fabbro, D., and Gray, N. S. (2006) Allosteric inhibitors of Bcr-abl-dependent cell proliferation. *Nat. Chem. Biol. 2*, 95–102.
50. Schindler, T., Sicheri, F., Pico, A., Gazit, A., Levitzki, A., and Kuriyan, J. (1999) Crystal structure of Hck in complex with a Src family-selective tyrosine kinase inhibitor. *Mol. Cell 3*, 639–648.